Accurate Nonlocal Impact Ionization Models for Conventional and Staircase Avalanche Photodiodes Derived by Full Band Monte Carlo Transport Simulations

Alessandro Pilotto, David Esseni, *Fellow, IEEE*, Luca Selmi, *Fellow, IEEE*, and Pierpaolo Palestri, *Senior Member, IEEE*

***Abstract*— We present a procedure to extract the nonlocal impact ionization coefficients in Avalanche Photodiodes (APDs) operating in the linear regime from Full Band Monte Carlo simulations. The Monte Carlo calculations have been calibrated on existing experimental data for GaAs p-i-n APDs with different thickness of the intrinsic region. Inspection of impact ionization generation rate in p-i-n and staircase GaAs APDs led us to identify the limitations of existing nonlocal-history dependent impact ionization models. The introduction of an energy dependent relaxation length for the computation of the effective fields significantly improves the model accuracy in predicting the gain and noise associated to conduction and valence band steps in staircase APDs without additional computational burden. This improved nonlocal-history dependent model is thus a powerful tool to design and optimize APDs with different architectures.**

***Index Terms*— Avalanche photodiodes, impact ionization, full band Monte Carlo.**

I. Introduction

ACCURATE modelling of impact ionization is of fundamental importance to study the static and dynamic performance of many electron devices and, notably, Avalanche Photodiodes (APDs) operating in the *linear* regime (i.e. biased below the breakdown voltage). Impact ionization models range from simple local analytical expressions [1], [2], where experimental impact ionization coefficients (α for electrons and β for holes) are fitted by exponential functions, all the way to Full Band Monte Carlo transport simulators [3], [4], [5], [6].

Manuscript received 23 May 2022; revised 18 July 2022; accepted 16 August 2022. Date of publication 22 August 2022; date of current version 2 September 2022. This work was supported by the Italian Ministero dell'Istruzione, Università e Ricerca (MIUR) through the Progetto di Rilevante Interesse Nazionale (PRIN) 2015 Project under Grant 2015WMZ5C8. *(Corresponding author: Pierpaolo Palestri.)*

Alessandro Pilotto was with the Dipartimento Politecnico di Ingegneria e Architettura, University of Udine, 33100 Udine, Italy. He is now with the Université Paris-Saclay, CNRS, Centre de Nanosciences et de Nanotechnologies, 91120 Palaiseau, France (e-mail: pilotto.alessandro@spes.uniud.it).

David Esseni and Pierpaolo Palestri are with the Dipartimento Politecnico di Ingegneria e Architettura, University of Udine, 33100 Udine, Italy (e-mail: palestri@uniud.it).

Luca Selmi is with the Dipartimento di Ingegneria "Enzo Ferrari," University of Modena and Reggio Emilia, 41100 Modena, Italy.

Color versions of one or more figures in this article are available at https://doi.org/10.1109/JQE.2022.3200728.

Digital Object Identifier 10.1109/JQE.2022.3200728

In between, the so-called Non-Local History-Dependent (NL-HD) impact ionization models (either based on the Dead Space approximation [7] or on effective fields [8], [9]) recently led to successful determination of the gain (M), the excess noise factor (F), and the time response of both conventional p-i-n APDs [7], [10], [11], [12] and staircase APDs [9], [13]. Similarly to local models, NL-HD models describe impact ionization at a macroscopic level, but α and β are functions of the generation (x) and the ionization (x') points and they depend on the whole electric field profile between x and x'. NL-HD models correctly reproduce the behavior of APDs (poorly described by local models) with a limited computational burden compared to Monte Carlo simulations. However, NL-HD models need to be calibrated on experimental measurements of M and F and they rely on approximations that limit their applicability, namely, they assume that electrons and holes only travel in the direction of the electric field and that carriers are generated by impact ionization with negligible kinetic energy.

In this work, Full Band Monte Carlo (FBMC) transport simulations have been used to investigate the limits of NL-HD models and, in particular, to understand when the underlying approximations lead to inaccurate results. The analysis of the NL-HD impact ionization coefficients' profiles extracted from FBMC transport simulations inspired the derivation of a new NL-HD model for accurate study of the gain and noise performance of conventional and staircase APDs.

This paper extends the preliminary investigation reported in [6] by providing many details on the FBMC transport simulator and on the procedure to extract from simulations the impact ionization rates, considering both conventional p-i-n APDs [11] and AlGaAs/GaAs-based superlattices [14], where pseudomorphic heterojunctions are exploited to increase the electron impact ionization probability with respect to the ionization probability of holes to reduce the excess noise factor at a given gain [15].

In particular, Section II summarizes the key features of the FBMC transport simulator used as reference in this work. Section III, reports the extraction of the nonlocal impact ionization coefficients, $\alpha(x|x')$ and $\beta(x|x')$, from FMBC transport simulations. In Section IV, we propose an improved

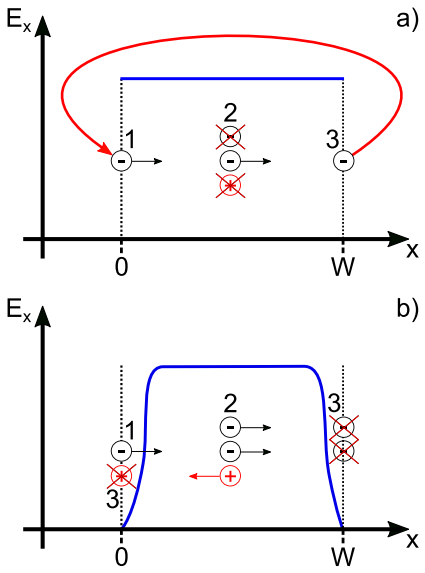

Fig. 1. Schematic representation of the boundary conditions applied to FBMC transport simulations throughout the paper. a) Looping boundary conditions with uniform electric field. b) Injecting boundary conditions with arbitrary electric field profile.

formulation of the NL-HD model of [9], featuring energy dependent relaxation lengths, to achieve a better match of the impact ionization coefficients with those computed by FBMC simulations, even in the presence of band discontinuities. The new model is then used to study the gain and noise characteristics of GaAs APDs, including devices featuring conduction band discontinuities. Finally, Section V reports our concluding remarks.

II. The Full Band Monte Carlo Transport Simulator

This Section provides a brief description of the most relevant features of the FBMC transport simulator that was developed and used throughout the paper. Details about the band structure, the scattering rates and their calibration can be found in Appendix I. In this work we will focus on GaAs based APDs, that are actively investigated for X-ray detection due to the large atomic number of GaAs. The FBMC can, in principle, be used for any other III-V compound semiconductor, if the correct parameters for the band structure and scattering mechanisms are available.

The FBMC transport solver moves electrons and holes according to the dynamic equations, described as a sequence of free flights interrupted by scattering events [16], consistently with the full band dispersion relation $E_n(\vec{k})$ [17]. A key aspect of FBMC transport simulations is the choice of the boundary conditions. Two of them have been used (Fig. 1), denoted in the following as *looping* (Fig. 1a) and *injecting* (Fig. 1b).

Looping boundary conditions apply to a uniform and infinite slab of bulk semiconductor with constant electric field. After an impact ionization event the secondary electron and hole are immediately removed from the simulation domain, so that statistics are computed by tracking only the primary electron (see event 2 in Fig. 1a). The simulation ends when a given number of free flights has occurred (e.g. 10^7).

Injecting boundary conditions for the contacts (i.e. electrons injected at $x = 0$ and holes at $x = W$) apply to an arbitrary electric field profile, possibly imported from TCAD simulations [18] of APD structures, that is kept frozen during the FBMC simulation, since the few electron-hole pairs produced by impact ionization events in a linear mode APD do not change appreciably the device electrostatics. After an impact ionization event, the positions in the real and reciprocal spaces of the primary and secondary carriers are tracked, and recursion is used to handle the increasing number of particles in the simulation domain [13]. When an electron reaches the right boundary ($x = W$), it is removed from the simulation domain, and the same happens for a hole reaching the left boundary at $x = 0$. The simulation consists of many trials (e.g. 10^5) each starting from a single electron injected at $x = 0$ (as in Fig. 1b) and ending when all carriers exit the simulation domain. Similar simulation flows occur when holes are injected at $x = W$.

A. Impact Ionization Under Uniform Electric Field

We have employed two alternative methods to extract the impact ionization coefficients in bulk GaAs (α and β for electrons and holes, respectively). Both methods are based on looping boundary conditions (Fig. 1a). In the first method, α and β are defined as the reciprocal of the average distance, $\langle l_e \rangle$ for electrons and $\langle l_h \rangle$ for holes, between consecutive impact ionization events, namely

$$\alpha = \frac{1}{\langle l_e \rangle}. \tag{1}$$

In the second method, instead, the impact ionization coefficients at a given electric field are computed from the energy-dependent impact ionization scattering rate $SR_{II,e}(E)$, the energy distribution function $F_{distr}(E)$, given by the FBMC as the number of electrons per energy bin normalized by the width of the energy bin, and the drift velocity v_e

$$\alpha = \frac{\int_0^{+\infty} SR_{II,e}(E) F_{distr}(E) dE}{v_e \int_0^{+\infty} F_{distr}(E) dE}. \tag{2}$$

Similar equations have been used to compute β.

Figure 2 compares the results of Eqs. 1 and 2 with the experiments of [19]. A good agreement between the two methods and with the data reported in [19] is achieved over the whole explored range of electric fields.

B. Model Validation for GaAs p-i-n APDs

We have validated the FBMC transport model with injecting boundary conditions by computing the gain $M = \langle m \rangle$ and the excess noise factor $F = \langle m^2 \rangle / M^2$, where m is the gain calculated in a trial, in a few GaAs p-i-n APDs. The electric field profiles were taken from TCAD simulations [18]. The results of FBMC simulations are compared with the experimental $M(V_{rev})$ and $F(M)$ curves of [11] in Fig. 3, showing a good mutual agreement using the doping and the dimensions reported in [11]. It is worth noting that in FBMC simulations no device property or parameter adjustment has been carried out, besides those necessary to match the experimental $v(E_x)$

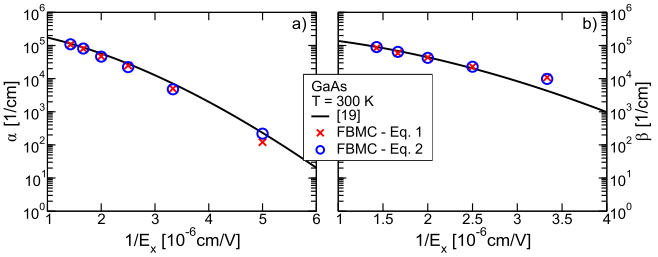

Fig. 2. a) α and b) β versus the reciprocal of the electric field in bulk GaAs at $T = 300$ K. FBMC simulations with looping boundary conditions (Fig. 1a) and Eq. 1 (red crosses) or Eq. 2 (blue solid line) are compared with experiments [19] (black solid).

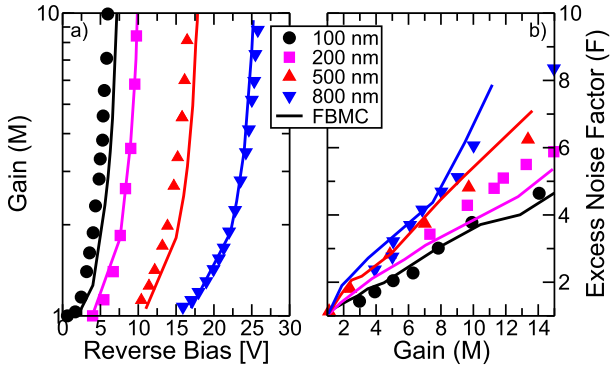

Fig. 3. a) M versus V_{rev} and b) F versus M curves for GaAs p-i-n APDs. FBMC with injecting boundary conditions and electric field profiles from TCAD [18] (solid lines) is compared with experiments [11] (symbols).

curves (see [6] and the calibration of the impact ionization scattering rates in Fig. 17).

III. Extraction of $\alpha(x|x')$ and $\beta(x|x')$ From FBMC Transport Simulations

As outlined in Section I, the impact ionization coefficients $\alpha(x|x')$ and $\beta(x|x')$ of NL-HD models are functions of both the generation and the ionization positions (x and x', respectively), and they depend on the whole electric field profile between x and x'. It is therefore clear that neither Eq. 1 nor Eq. 2 are suited to extract $\alpha(x|x')$ and $\beta(x|x')$ from FBMC simulations. For this reason, in [6] we have derived the expression reported in Eq. 3, as shown at the bottom of the page, that can been applied to FBMC simulations of p-i-n APDs (with injecting boundary conditions, see Fig. 1b) after discretization of the multiplication region with a uniform mesh of spacing Δx. The denominator of Eq. 3 counts all electrons generated in x that ionize in $[0, x' - \Delta x/2]$, and not only those in the $[x, x' - \Delta x/2]$ interval. This includes electrons that, due to a scattering event, travel with negative velocity and ionize at points lying before the carrier generation point. It is worth noting that Eq. 3 extends the approach proposed

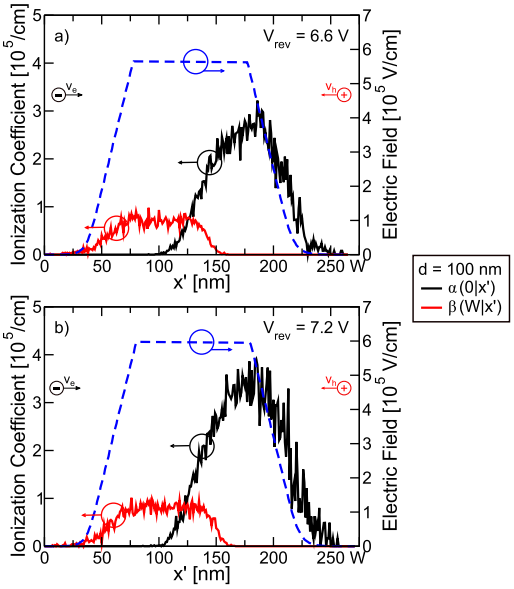

Fig. 4. $\alpha(0|x')$ (black) and $\beta(W|x')$ (red) computed with FBMC simulations by using Eq. 3 and injecting boundary conditions (Fig. 1b) in a GaAs p-i-n APD with nominal thickness of the intrinsic region equal to $d = 100$ nm. Electrons are injected at $x = 0$ and drift from left to right, while holes are injected at $x = W$ and drift from right to left. The electric field profiles (blue) have been extracted from TCAD simulations [18] at a) $V_{rev} = 6.6$ V or b) $V_{rev} = 7.2$ V.

in [20], where the nonlocal impact ionization coefficients were extracted by means of FBMC simulations without taking into account the history of the carriers. In [20], all the ionization events induced by electrons injected/generated from $x = 0$ to $x = x'$ and by holes injected/generated from $x = x'$ to $x = W$ are collapsed together, so that only the ionization position x' is considered.

Using Eq. 3 for the 100 nm-thick p-i-n APD of Fig. 3, yields the results in Fig. 4. Two reverse bias voltages are considered, one electron is injected at $x = 0$ and one hole at $x = W$. We notice that both $\alpha(x|x')$ and $\beta(x|x')$ reach their peak inside the high field (depletion) region of the APD and then rapidly decay to zero as soon as the field decreases.

Figure 5 compares the $M(V_{rev})$ and $F(V_{rev})$ for GaAs p-i-n diodes computed with FBMC simulations (same results already reported in Fig. 3) with those obtained with the NL-HD model [8], [9] by using as input the impact ionization coefficients extracted from the very same FBMC simulations. Although the two methods give very similar trends, a point by point comparison at fixed bias voltage shows that the FBMC and the NL-HD model give exactly the same results only at low gains, while discrepancies can be noticed at high gains, especially in short devices ($\simeq$ 20% for M and F of the $d = 100$ nm device at $V_{rev} = 7.4$ V). The reasons of this behavior will be better understood by analyzing the results reported in Section III-A.

$$\alpha(x|x') = \frac{\textit{No. of electrons generated in } x \textit{ (by II or a photon) that ionize in } x' \pm \Delta x/2}{\Delta x \cdot \left(\textit{No. of electrons generated in } x - \textit{No. of electrons generated in } x \textit{ that ionize in } [0, x' - \Delta x/2)\right)} \quad (3)$$

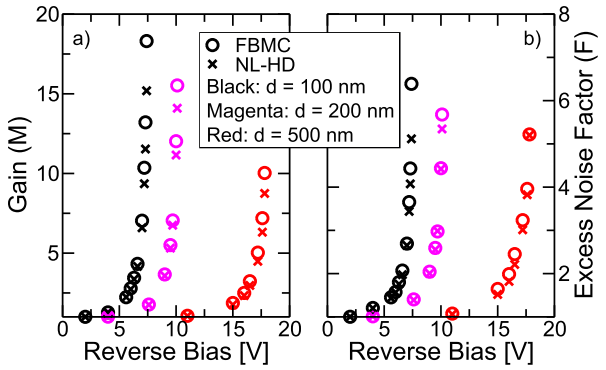

Fig. 5. Comparison between a) M and b) F versus V_{rev} curves for GaAs p-i-n diodes computed with the FBMC simulations of Fig. 3 and the ones obtained by using the NL-HD model equations [8], [9] when the $\alpha(x|x')$ and $\beta(x|x')$ extracted from FBMC simulations, with Eq. 3 and injecting boundary conditions, are used as inputs of the NL-HD model (crosses).

A. GaAs p-i-n APDs With Uniform Electric Field Profiles

In this Section we investigate the NL-HD impact ionization coefficients, and, in particular, we explain why the equations of NL-HD models do not give the exact same results as FBMC simulations, not even if $\alpha(x|x')$ and $\beta(x|x')$ extracted from FBMC simulations are used (see Fig. 5). To this purpose, we examine the results of using Eq. 3 for a GaAs p-i-n APD with uniform electric field, so as to rule out possible effects of the field non-uniformity close to the boundaries, which are relatively more relevant in thin devices. Such a simplified simulation setup also allows us to compare FBMC simulations when either looping (Fig. 1a) or injecting (Fig. 1b) boundary conditions are employed.

To this end, we set the device thickness equal to the width of the high field region and we applied injecting boundary conditions (Fig. 1b) for different values of the uniform electric field. Sample results for $d = 100$ nm are shown in Fig. 6 for an electron generated at $x = 0$ (Fig. 6a) or at $x = 50$ nm (Fig. 6b), and in Fig. 7 for a hole generated at $x = 100$ nm (Fig. 7a) or at $x = 50$ nm (Fig. 7b). We see that $\alpha(x|x')$ and $\beta(x|x')$ saturate to a constant value (in the following denoted as α^* and β^*, respectively) after few tens of nanometers from the injection point, but α^* and β^* differ from the α and β obtained as a function of the field by using Eqs. 1 and 2 (see Fig. 2 and the dashed lines in Figs. 6 and 7), since those equations apply only to looping boundary conditions (Fig. 1a). In fact, as explained in [21], α^* and β^* are the impact ionization coefficients for an electron and a hole that have traveled over their dead space d_e and d_h, respectively.[1]

Figure 6b shows that at high reverse bias voltages (namely at high gains) $\alpha(x|x') > 0$ also for $x' < x$. This may happen for two different reasons: an electron can travel with negative velocity because of a previous as *backscattering* event, or because it was generated by impact ionization with nonzero kinetic energy and negative velocity. At high electric fields, electrons need to travel across short distances to gain an energy sufficient for their ionization, especially if they are generated by energetic carriers, and this may result in impact ionization events also for $x' < x$. On the other hand, by looking at Fig. 7, we notice that, with the calibration used in this paper, hole impact ionization for $x' > x$ is negligible. In practice, for linear mode APDs, the fact that electrons can ionize also for $x' < x$ has the effect of increasing the randomness of the impact ionization process and, thus, it translates into a slight increase of both the gain and the excess noise factor at a given electric field. The discrepancy between the NL-HD models and FBMC results reported in Fig. 5 can be explained by recalling that NL-HD equations assume that carriers travel only in the direction of the electric field and, moreover, that secondary carriers originating from an impact ionization event are generated with negligible kinetic energy.

As it can be observed in Figs. 6b and 7b, the main limitation to the use of Eq. 3 is that FBMC simulations become computationally demanding if one needs to extract smooth profiles for the history dependent impact ionization coefficients, $\alpha(x|x')$ and $\beta(x|x')$, for the secondary carriers (i.e. $x > 0$ for electrons and $x < W$ for holes). This requires to simulate the evolution of an extremely large number of particles. For instance, on a cluster with 40 cores and 190 GB of RAM, the simulation of 10^5 trials for a single bias point takes from two hours to one week, depending on the device thickness and on the applied

[1]The dead space is defined as the distance that a carrier has to travel to gain an energy that is sufficient to trigger impact ionization [7].

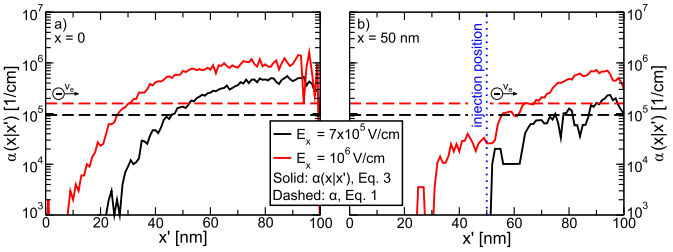

Fig. 6. $\alpha(x|x')$ extracted from FBMC simulations by using Eq. 3 and injecting boundary conditions (Fig. 1b) in a 100 nm-thick GaAs p-i-n APD with electron injection from the left side at $E_x = 7 \times 10^5$ V/cm (black) and $E_x = 10^6$ V/cm (red). The electron is generated either at a) $x = 0$ or at b) $x = 50$ nm. The dashed lines represent $\alpha(E_x)$ computed by using FBMC simulations by using Eq. 1 and looping boundary conditions (Fig. 1a).

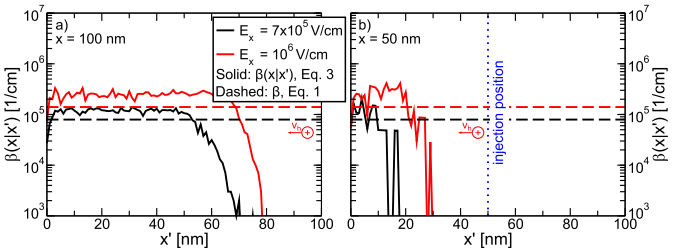

Fig. 7. $\beta(x|x')$ extracted from FBMC simulations by using Eq. 3 and injecting boundary conditions (Fig. 1b) in a 100 nm-thick GaAs p-i-n APD with hole injection from the right side at $E_x = 7 \times 10^5$ V/cm (black) and $E_x = 10^6$ V/cm (red). The hole is generated either at a) $x = 0$ or at b) $x = 50$ nm. The dashed lines represent $\beta(E_x)$ computed by using FBMC simulations Eq. 1 and looping boundary conditions (Fig. 1a).

bias voltage (thick devices with large multiplication are the most demanding).

B. Threshold Energies for Impact Ionization and PDFs of the Distance Between Ionization Events

The results of the simulations performed in Section III-A can be exploited to compute the electron and hole threshold energies for impact ionization in GaAs. In fact, in the framework of the Dead Space model [7], we can write the probability density function for the distance between consecutive electron impact ionization events, $PDF(l_e)$, as

$$PDF(l_e) = \begin{cases} 0, & l_e < d_e \\ \alpha^* e^{-\alpha^*(l_e - d_e)}, & l_e \geq d_e \end{cases}, \tag{4}$$

therefore

$$\frac{1}{\alpha} = \langle l_e \rangle = \int_{d_e}^{\infty} l_e \alpha^* e^{-\alpha^*(l_e - d_e)} dl_e = d_e + \frac{1}{\alpha^*}, \tag{5}$$

and similar equations hold also for holes. By comparing the values of α and β with the values of α^* and β^* computedwith FBMC simulations by using looping (Fig. 1a) and injecting (Fig. 1b) boundary conditions, respectively, we have found that d_e can be expressed as $d_e = E_{th,e}/qE_x$, where $E_{th,e} = 4.25$ eV, while d_h can be written as $E_{th,h}/qE_x$, with $E_{th,h} = 3.0$ eV. We notice that the adopted calibration (Fig. 17) leads to an $E_{th,e}$ larger than the corresponding value reported in [21] ($E_{th,e} = 3.0$ eV). Our results, however, agree with the outcome of Full Band Monte Carlo simulations in [22], reporting a distribution for the electron energy before impact ionization centered at 4 eV. On the other hand, the value of $E_{th,h}$ that we have computed is in close agreement both with [21] ($E_{th,h} = 3.3$ eV) and with [22], with the second reference reporting a distribution of the hole energy before ionization centered at 3 eV. Similarly to what has been done in [4] and [23], FBMC simulations with looping boundary conditions (Fig. 1a) can also be used to compute the probability density functions $PDF(l_e)$ and $PDF(l_h)$ of l_e and l_h, respectively, at a given electric field.

Figures 8 and 9 compare the $PDF(l_e)$ computed with FBMC simulations with the one predicted by the Dead Space model with $E_{th,e} = 4.25$ eV (Eq. 4). In Fig. 8 secondary electrons are generated with an initial energy derived from the computation of the impact ionization scattering rate (Eq. 11). In the simulations reported in Fig. 9, instead, we have imposed that secondary carriers are always generated with null kinetic energy, so as to be fully consistent with the assumptions of the NL-HD models.

The agreement between Eq. 4 and FBMC results is good for all values of electric field both in Fig. 8 and 9; however, when secondary electrons are generated with a non-null initial energy (Fig. 8), $PDF(l_e)$ is greater than zero also for $l_e < d_e$, particularly at large applied electric fields. This is consistent with the fact that, due to backscattering or to an initial negative velocity, some energetic electrons can ionize also at position $x' < x$ (see Fig. 6).

A similar analysis has been carried out also for holes and it is illustrated in Figs. 10 and 11, which show $PDF(l_h)$ when

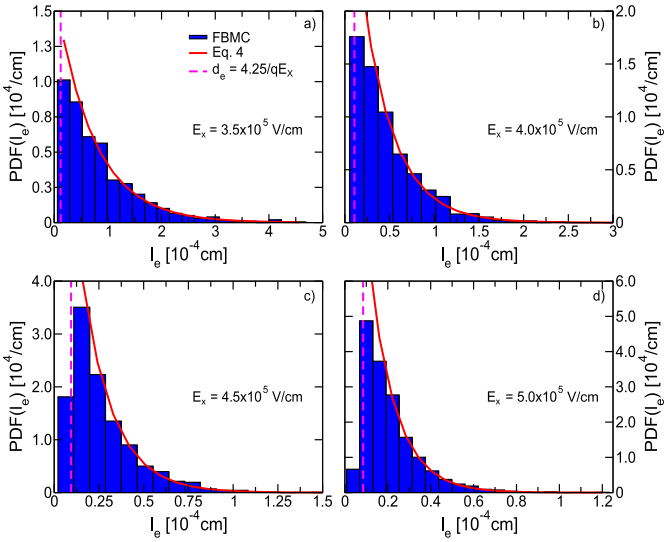

Fig. 8. $PDF(l_e)$ at different electric fields. Results of FBMC simulations with looping boundary conditions (Fig. 1a) (blue) are compared with Eq. 4 (red). The magenta dashed line is $d_e = E_{th,e}/qE_x$, with $E_{th,e} = 4.25$ eV, as extracted by comparing α and α^* computed with FBMC simulations by using looping and injecting boundary conditions, respectively (Eq. 5). The electric field is a) $E_x = 3.5 \times 10^5$ V/cm, b) $E_x = 4.0 \times 10^5$ V/cm, c) 4.5×10^5 V/cm, and d) $E_C = 5.0 \times 10^5$ V/cm.

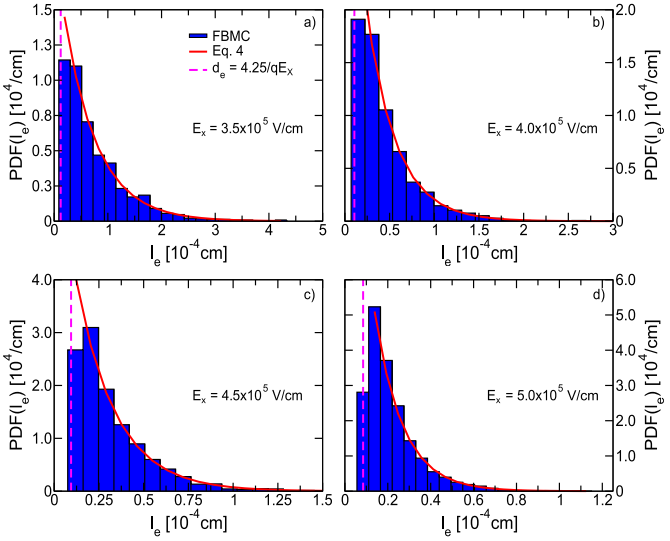

Fig. 9. Same as Fig. 8, but secondary electrons are generated with null kinetic energy in FBMC simulations.

secondary holes are generated according to Eq. 11, and when, after an impact ionization event, secondary holes are generated with null kinetic energy.

The comparison with the analytical $PDF(l_h)$ predicted by the Dead Space model of [7] (Eq. 4 substituting α^* with β^* and d_e with d_h) has been performed by setting $E_{th,h} = 3.0$ eV, as extracted by comparing β and β^* computed with FBMC simulations and using looping and injecting boundary conditions, respectively (Eq. 5). Good agreement is once again obtained. We notice that in Figs. 10 and 11, the first filled bin in the histograms is always the one after d_h, indicating that, in GaAs and for these electric fields, hole's impact ionization

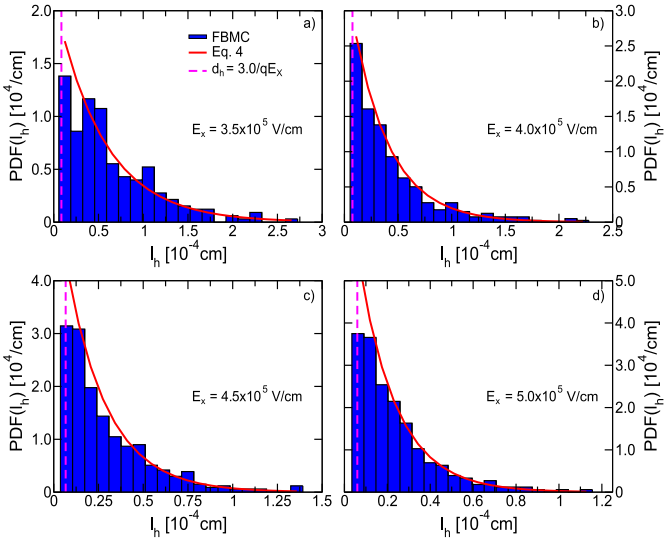

Fig. 10. $PDF(l_h)$ at different electric fields. Results of FBMC simulations with looping boundary conditions (Fig. 1a) (blue) are compared with Eq. 4 (red). The magenta dashed line is $d_h = E_{th,h}/qE_x$, with $E_{th,e} = 3.0$ eV, as extracted by comparing β and β^* computed with FBMC simulations by using looping nad injecting boundary conditions, respectively (Eq. 5). The electric field is a) $E_x = 3.5 \times 10^5$ V/cm, b) $E_x = 4.0 \times 10^5$ V/cm, c) 4.5×10^5 V/cm, and d) $E_C = 5.0 \times 10^5$ V/cm.

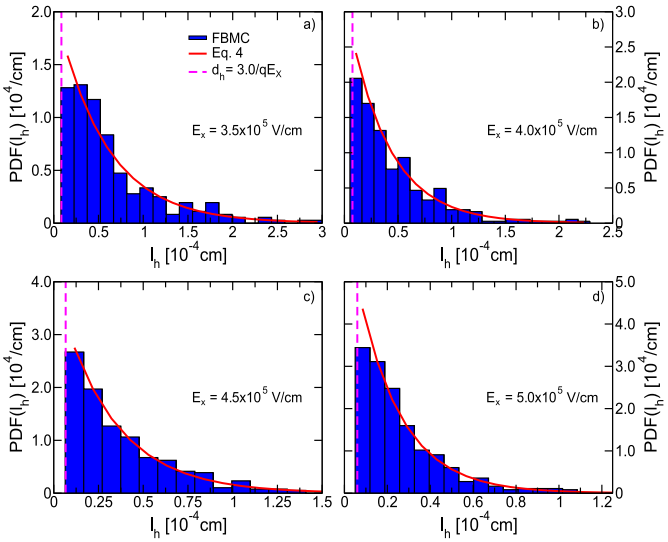

Fig. 11. Same as Fig. 10, but secondary holes are generated with null kinetic energy in FBMC simulations.

is less sensitive than electron's impact ionization to the initial energy of the secondary carrier.

IV. EBHDM With Energy Dependent Relaxation Lengths

In this Section, we show how the results for the electron's and hole's impact ionization coefficients, $\alpha(x|x')$ and $\beta(x|x')$, obtained with FBMC simulations have been used to improve the NL-HD impact ionization model described in [9]. Our final goal is to model the impact ionization coefficients in the presence of a conduction band discontinuity and for low applied electric fields, so as to evaluate the performance of a single step AlGaAs/GaAs-based staircase APDs [14], [24].

TABLE I

Comparison Between the Nonlocal Impact Ionization Parameters for GaAs Used in [9] and the Ones Used in the New Model Developed in This Work

	A_e [10^6/cm]	E_{ce} [10^6V/cm]	γ_e	λ_e [nm]
[9]	3.30	1.75	1.0	18
New Model	7.06	1.97	1.0	Eq. 10, Tab. II

	A_h [10^6/cm]	E_{ch} [10^6V/cm]	γ_h	λ_h [nm]
[9]	0.73	1.42	1.0	24
New Model	0.95	1.42	1.0	Eq. 10, Tab. II

We recall that, in the NL-HD model of [9], the position dependent impact ionization coefficients are expressed as

$$\alpha(x|x') = A_e exp\left[-\left(\frac{E_{ce}}{E_{eff,e}(x|x')}\right)^{\gamma_e}\right] \quad (6)$$

$$\beta(x|x') = A_h exp\left[-\left(\frac{E_{ch}}{E_{eff,h}(x|x')}\right)^{\gamma_h}\right], \quad (7)$$

where $E_{eff,e}(x|x')$ and $E_{eff,h}(x|x')$ are the electron and hole effective fields, respectively, that are linked to the quasi-electric fields by the general relations

$$E_{eff,e}(x|x') = \int_x^{x'} \frac{1}{\lambda_e(x|x'')} \frac{dE_C}{dx''} \exp\left(\frac{x''-x'}{\lambda_e(x|x'')}\right) dx'', \quad (8)$$

$$E_{eff,h}(x|x') = \int_{x'}^{x} \frac{1}{\lambda_h(x|x')} \frac{dE_V(x'')}{dx''} exp\left(\frac{x'-x''}{\lambda_h(x|x')}\right) dx'', \quad (9)$$

where $E_C(x)$ and $E_V(x)$ are the conduction and valence band profiles, respectively. Differently from [9], where the relaxation lengths λ_e and λ_h are constant, in this work we propose a novel formulation for $\lambda_e(x|x')$ and $\lambda_h(x|x')$ by linking their value to the effective field (which is an indication of the carrier's energy). By experimenting with different functional forms, we have found a suitable expression for $\lambda_{e,h}(x|x')$ that reproduces the results of FBMC simulations:

$$\lambda_{e,h}(x|x') = \frac{A_{\lambda e,h}}{B_{\lambda e,h} + E_{eff,e,h}(x|x')}. \quad (10)$$

We have calibrated the the values of A_e, A_h, E_{ce}, E_{ch}, γ_e and γ_h to insert into Eqs. 6 and 7 that best fit the curves of α^* and β^* as a function of the reciprocal of the electric field given by the FBMC simulations in Section III, at uniform electric field, and with injecting boundary conditions[2] (Fig. 1b). A comparison between the model parameters for GaAs used in [9] and the ones of this work is reported in Tab. I, while the parameters $A_{\lambda e,h}$ and $B_{\lambda e,h}$ to insert into Eq. 10 are reported in Tab. II.

Figures 12 and 13 compare the profiles of $\alpha(0|x')$ and $\beta(d|x')$ in a $d = 200$ nm-thick GaAs p-i-n APD obtained with FBMC simulations with injecting boundary conditions (Fig. 1b), with the position dependent impact ionization coefficients corresponding to different approximations, namely the Dead Space model [7] calibrated on the results of Section III

[2]We remark that, even if the electric field in the considered structure is uniform, injecting boundary conditions have to be applied, since injecting boundary conditions can be employed only for the simulation of an infinitely long slab of bulk semiconductor.

TABLE II

VALUES OF THE PARAMETERS $A_{\lambda e,h}$ AND $B_{\lambda e,h}$ TO INSERT INTO EQ. 10 TO COMPUTE THE ENERGY DEPENDENT RELAXATION LENGTHS, $\lambda_{e,h}(x|x')$, FOR ELECTRONS AND HOLES

$A_{\lambda e}$ [V]	$B_{\lambda e}$ [10^5 V/cm]
1.41	1.32

$A_{\lambda h}$ [V]	$B_{\lambda h}$ [10^5 V/cm]
0.61	0.15

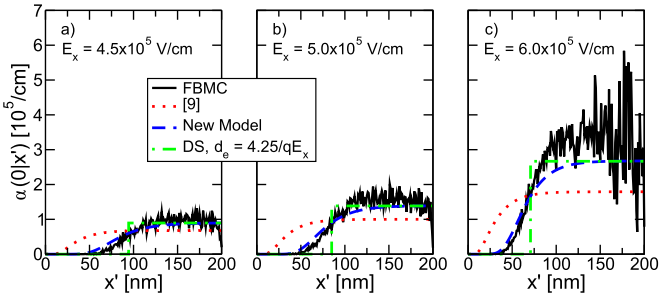

Fig. 12. $\alpha(0|x')$ for a 200 nm-thick GaAs p-i-n diode. FBMC simulations with injecting boundary conditions (Fig. 1b) (black solid line) are compared with the NL-HD model of [9], with the new model developed in this work (blue dashed line), and with the Dead Space model (DS) calibrated on the FBMC results reported in Section III ($d_e = 4.25/qE_x$, green dashed-dotted line). The electric field is a) $E_x = 4.5 \times 10^5$ V/cm, b) $E_x = 5.0 \times 10^5$ V/cm, and c) 6.0×10^5 V/cm.

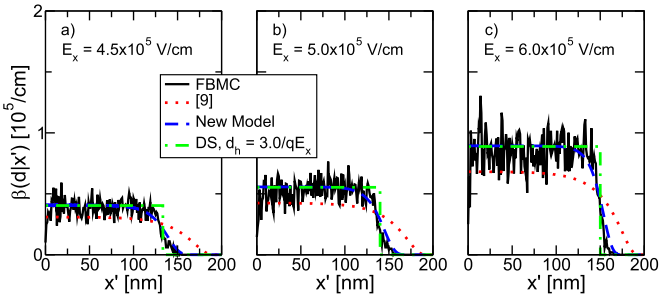

Fig. 13. Same as Fig. 12, but for $\beta(d|x')$. For the Dead Space model $d_h = 3.0/qE_x$.

($d_e = 4.25/qE_x$ and $d_h = 3.0/qE_x$), the NL-HD model presented in [9], and the new implementation of the same model with energy dependent relaxation lengths. The new model for $\alpha(x|x')$ and $\beta(x|x')$ provides the best agreement with the reference FBMC results among all curves. Notice that the model in [9] is not calibrated on FBMC simulations, but on the experimental M and F of GaAs p-i-n APDs, while the Dead Space model is calibrated on the results of the FBMC simulations of Section III, but nevertheless fails to capture the soft threshold behavior of the $\alpha(x|x')$ and $\beta(x|x')$ profiles.

A. Application to GaAs p-i-n APDs

As a first check of the new model proposed in Section IV, we have computed the $M(V_{rev})$ and $F(M)$ curves for GaAs p-i-n APDs previously reported in Fig. 3. Figure 14 compares the new results to the NL-HD model of [9] and the reference FBMC simulations. The same electric field profiles used in Fig. 3 have been fed to all models.

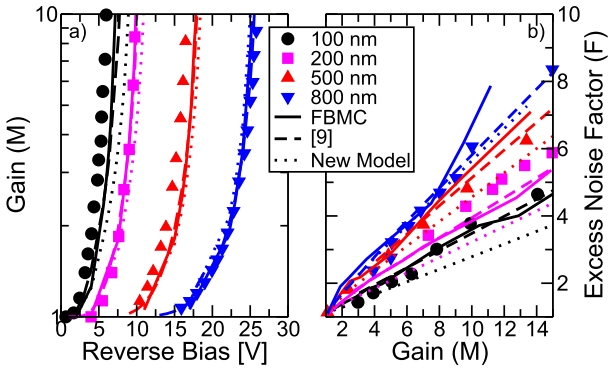

Fig. 14. Comparison between the a) $M(V_{rev})$ and b) $F(M)$ curves reported in Fig. 3, the results of the NL-HD of [9], and the new model with energy dependent relaxation lengths (dotted lines).

We notice that the new model is in fairly good agreement with the experimental results for the $M(V_{rev})$ curves for all the simulated devices. As for the excess noise factor, the $F(M)$ curves of the 500 nm and 800 nm-thick diodes are matched quite well, while the ones of the 100 nm and 200 nm-thick diodes are slightly underestimated. This is not unexpected for the following reason: consider that finding an expression for $\lambda(x|x')$ and model parameters that work for all x, x' points is not trivial. The target of the calibration procedure was thus to reproduce the $\alpha(0|x')$ and $\beta(d|x')$ profiles extracted from FBMC simulations with injecting boundary conditions (Fig. 1b), i.e. the profiles that describe the behavior of carriers generated by the absorption of a photon outisde the high field region of the APD, while no tests were performed for electrons and holes injected/generated at positions different from respectively $x = 0$ and $x = d$. Therefore, after calibration we found that with Eq. 10 and the parameters proposed in Tab. II, it is not always possible to accurately predict $\alpha(x|x')$ and $\beta(x|x')$ for arbitary values of x, i.e. to descibe the behavior of carriers generated inside the high field region by impact ionization. These carriers have an impact on M and F at high gain for short devices. Even though this problem may be assessed in a future work, the agreement in Fig. 14 between the experiments and the results of the new NL-HD model is within 20%, as opposed to 13% of the model of [9]. Moreover, we recall that the model calibration in [9] was focused on the experimental results in Fig. 14 for M and F of GaAs p-i-n APDs. The calibration of the new NL-HD model of this work is instead more general, and it has an extended range of validity with respect to [9], as it will be shown in Section IV-B.

B. Application to Conduction Band Steps

Finally, we examined the behavior of GaAs APDs preceded by a single conduction band step of variable amplitude ΔE_C. To capture the basic physics of the process we have described the conduction band step as a contribution to the initial energy of the electron injected at $x = 0$, namely the initial energy of the injected electron is set to ΔE_C.

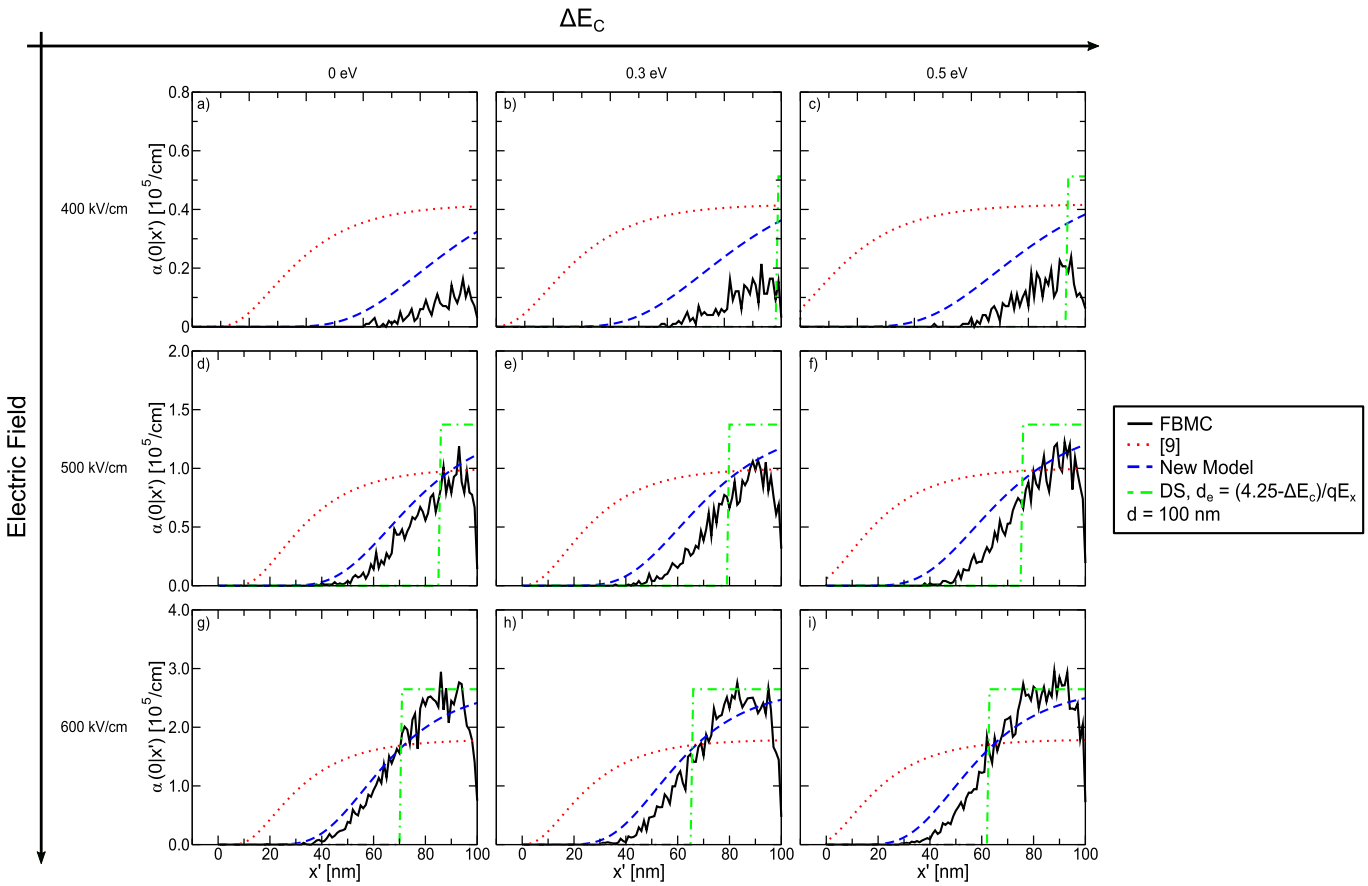

Fig. 15. $\alpha(0|x')$ for a 100 nm-thick GaAs device preceded by conduction band steps of different amplitudes and for different values of the applied electric field. FBMC simulations obtained by applying injecting boundary conditions (Fig. 1b) (black solid line) are compared with the NL-HD model of [9], with the new NL-HD model with energy dependent relaxation lengths proposed in this work (blue dotted line), and with the Dead Space model (DS) calibrated on the FBMC results reported in Section III, where $d_e = (4.25 - \Delta E_C)/qE_x$ (green dashed-dotted line). The plots a) to g) correspond to different combinations of ΔE_C (see label on top) and electric field (see label on the left).

The simulated devices feature $d = 100$ nm and $\Delta E_C = 0$, 0.3 eV, 0.5 eV (these values are consistent with the conduction band step at a $Al_xGa_{1-x}As$/GaAs heterojunction in a staircase APD [14], [24], where $\Delta E_C \simeq 0.355$ eV for $x = 0.45$ [25], [26]. Moreover, we have always applied an electric field along the x direction, $E_x = 400$, 500 and 600 kV/cm, to ensure that all the carriers exit from the simulation domain. For all the simulations, since in GaAs/AlGaAs staircase APDs as the ones in [14] and [24] impact ionization mostly takes place in GaAs layers (due to its lower band gap w.r.t. AlGaAs), parameters for GaAs have been used.

Figure 15 compares the profiles of $\alpha(0|x')$ obtained with the FBMC simulator for the 100 nm thick device with the profiles from the NL-HD model of [9], from the new NL-HD model with energy dependent relaxation lengths, and from the Dead Space model calibrated on the FBMC results of Section III. The electron dead space d_e is computed by subtracting the conduction band step to the threshold energy, namely $d_e = (4.25 - \Delta E_C)/qE_x$. We notice that the NL-HD model of [9] always overestimates the electron's impact ionization coefficients extracted from FBMC simulations, which are instead in good agreement with the new NL-HD model proposed in this paper. Interestingly, we also notice that the Dead Space model is not able to correctly reproduce the behavior of $\alpha(0|x')$ for structures that feature conduction band discontinuities, especially for low values of the applied electric field, where d_e is larger than (Fig. 15a) or comparable to the length of the device (Fig. 15b-e). Moreover, Fig. 15 shows that the peak value of the electron's impact ionization coefficient increases as either ΔE_C or the electric field increase. However, the largest variations of $\alpha(0|x')$ are found by increasing the applied electric field, suggesting that the conduction band discontinuities up to $\Delta E_C = 0.5$ eV are not sufficient to significantly boost of the gain. This is confirmed also by the results in Fig. 16, that compare the gain and the excess noise factor as a function of the applied electric field for the same devices of Fig. 15, and where we notice that a significant increase of the gain can be achieved only by increasing the electric field.

However, Fig. 16 shows that, with respect to FBMC simulations, the NL-HD model of [9] overestimates both the gain and the excess noise factor, while calculations with the new NL-HD model almost coincide with those of the FBMC, in the entire range of electric field values. This indicates that the new NL-HD model can be safely used to study the gain and excess noise factor of GaAs-based APDs over a wide range of electric fields also if we assume that carriers are injected in the simulation domain with nonzero kinetic energy, as in

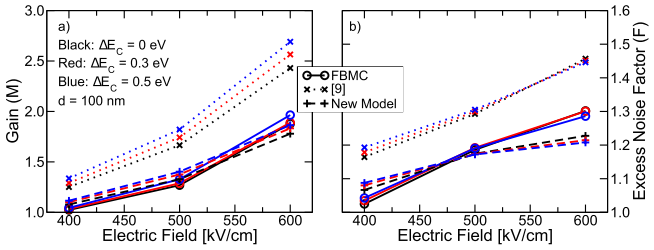

Fig. 16. Comparison between a) the gain and b) the excess noise factor as a function of the applied electric field and for different values of ΔE_C computed with the FBMC simulator (circles and solid lines) and with the EBHDM of [9] by using the parameters reported in [9] (crosses and dotted lines) or the ones reported in Tab. I with energy dependent relaxation lengths $\lambda_e(x|x')$ and $\lambda_h(x|x')$ (Eq. 10) (plus signs and dashed lines).

the case of staircase APDs at the start of each conduction or valence band step.

A comparison between experimental data for the gain and excess noise factor of AlGaAs/GaAs staircase APDs and the results of the NL-HD model proposed in this work (with the parameters of Tabs. I and II) has been recently published in [27].

V. Conclusion

We have derived a novel methodology based on Full Band Monte Carlo simulations to extract the position dependent impact ionization coefficients, and to assess the validity of Non-Local History-Dependent (NL-HD) impact ionization models. Inspection of the $\alpha(x|x')$ and $\beta(x|x')$ profiles lead us to propose an improved formulation, with energy dependent relaxation lengths to compute the effective fields for the NL-HD model presented in [9]. After calibration, the new model showed results in good agreement with FBMC simulations, which extend the range of validity of previous NL-HD models, for both conventional GaAs p-i-n APDs, and for devices with conduction band discontinuities as those in AlGaAs/GaAs staircase APDs.

However, other limitations of NL-HD models have been pointed out. Among them, one should consider that in NL-HD models secondary carriers are generated with zero kinetic energy and move only in the direction of the applied electric field. Therefore NL-HD models can be inaccurate at high gains in thin devices, when both the above simplifying assumptions become questionable. To the best of our knowledge, a way to circumvent this latter problem has not been found so far.

In this work, we focused on GaAs, but the proposed procedure can be used for the study of APDs based on other semiconductor materials. The calibration of the FBMC transport simulator requires experimental results for the drift velocity as a function of the electric field, and for the impact ionization coefficients in the bulk materials (data that are available for most of the materials of interest). Experimental measurements of the gain and the excess noise factor in APDs with different thicknesses are finally needed for a further tuning of the impact ionization model in the FBMC transport simulator. The NL-HD model, instead, is calibrated against the results of FBMC simulations.

TABLE III

Empirical Pseudopotential and Spin Orbit Interaction Parameters for GaAs Used in This Work. Please Refer to [17], [32], [33] for the Meaning of the Different Terms

$V_S(\sqrt{3})$ [Ry]	$V_S(\sqrt{4})$ [Ry]	$V_S(\sqrt{8})$ [Ry]	$V_S(\sqrt{11})$ [Ry]
-0.23	0	0.01	0.055
$V_A(\sqrt{3})$ [Ry]	$V_A(\sqrt{4})$ [Ry]	$V_A(\sqrt{8})$ [Ry]	$V_A(\sqrt{11})$ [Ry]
0.07	0.05	0	0.01

a_0 [m]	E_g [eV]	ζ	μ [Ry]	α
0.564×10^{-9}	1.424	5.34	0.0008	1.37

We have compared the NL-HD model and FBMC simulations in the case of electric field profiles that are essentially box like (i.e. uniform over a limited distance), and on staircase structures where the quasi-field is a combination of a box profile over the whole multiplication region and a Dirac-delta at each heterojunction. We thus believe that the NL-HD model, being in good agreement with the FBMC results for these two cases, can also reproduce well other field profiles, such as the triangular electric field profiles representative of pn junctions.

We can conclude that FBMC simulations are useful not only to simulate APDs but also to validate simpler and more efficient modelling approaches. For instance, the use of NL-HD impact ionization models based on the results of FBMC simulations combined with algorithms like the one in [13] allows us to study, with increased accuracy, the dynamic behavior of APDs based on heterostructures. All these simulation tools can contribute to develop of novel APD's architectures based on heterojunctions between compound semiconductors and their alloys [28], [29], [30] and possibly integrated on Silicon substrates [31].

Appendix I
Details About the Full Band Monte Carlo Transport Simulator

The full band dispersion relation $E_n(\vec{k})$ has been computed with the Local Empirical Pseudopotentials method [17] with form factors from [32] (see Tab. III). Four valence bands and four conduction bands have been considered in the calculations. Spin Orbit Interaction has been included as described in [33] (with the parameters in Tab. III) so that, in total, each simulation accounts for eight bands with spin-up and eight with spin-down.

The scattering rates with acoustic, polar optical and non-polar optical phonons have been computed by using the expressions reported in [32], and, due to the isotropic nature of GaAs, we have embraced the constant matrix element approximation to calculate the electron's and hole's impact ionization scattering rates [34]. Beside the impact ionization scattering rates, we also compute the energy distribution of the secondary electrons and holes $E_{e,e}(E_i, E_f)$ and $E_{h,e}(E_i, E_f)$ in the case of electron's ionization and $E_{h,h}(E_i, E_f)$ and $E_{e,h}(E_i, E_f)$ in the case of hole's ionization, that are needed to assign to the generated particles the appropriate energy E_f for any given energy of the primary carrier E_i. The scattering rates are stored as a function of the band index n, and of the $\vec{k}$-vector of the initial state inside the Irreducible

TABLE IV

SCATTERING PARAMETERS FOR GaAs USED IN THIS WORK: ρ IS THE DENSITY, c_l AND c_t ARE THE SOUND VELOCITIES RESPECTIVELY IN THE LONGITUDINAL AND TRANSVERSE DIRECTIONS, ε_0 AND ε_{infty} ARE RESPECTIVELY THE LOW AND HIGH FREQUENCY DIELECTRIC CONSTANTS, D_{ac} AND ΔK_{op} ARE THE DEFORMATION POTENTIALS FOR SCATTERING WITH ACOUSTIC AND NON-POLAR OPTICAL PHONONS, AND T_{ii} IS THE MATRIX ELEMENT FOR THE COMPUTATION OF THE IMPACT IONIZATION SCATTERING RATES. IN THE TABLE, THE SUBSCRIPTS h AND e REFER TO HOLES AND ELECTRONS, RESPECTIVELY

ρ [kg/m^3]	c_l [m/s]	c_t [m/s]	ϵ_0	ϵ_∞
5360	5240	3340	12.9	10.92

$D_{ac,h}$ [eV]	$\Delta K_{op,h}$ [eV/m]	$D_{ac,e}$ [eV]	$\Delta K_{op,e}$ [eV/m]
4.5	6.1×10^{10}	7.1	2.1×10^{10}

$T_{ii,h}$ [J/s]	$T_{ii,e}$ [J/s]
4.5×10^{-6}	8.0×10^{-7}

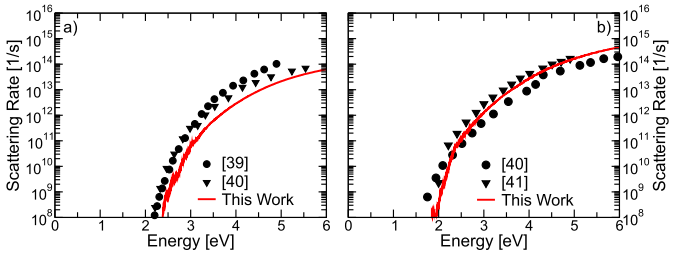

Fig. 17. a) Electron's and b) hole's impact ionization scattering rates in GaAs as a function of energy at $T = 300$ K. Our calculations (red lines), obtained by using the constant matrix element approximation [34], are compared with the results by other authors [39], [40], [41].

Wedge of the First Brillouin Zone (FBZ). At the end of any free flight the scattering mechanism (carrier-phonon, impact ionization or self-scattering) is randomly chosen according to the corresponding weight of that given scattering mechanism on the total scattering rate for the initial state $(n, \vec{k})$. For carrier-phonon scattering, a rejection technique is employed to select the state after scattering, while for impact ionization the new state is chosen randomly according to the energy distributions of secondary carrier. For instance, in the case of electron initiated impact ionization, the probability for a primary carrier with energy E_i to generate a secondary electron with energy E_f is

$$p(E_i, E_f) = \frac{E_{e,e}(E_i, E_f)}{\sum_{E_f} E_{e,e}(E_i, E_f)}. \tag{11}$$

Cumulative probabilities are computed for all the possible final energies and the generation of a random number $r \in [0, 1]$ is used to determine E_f. A final state at energy E_f in the FBZ is randomly selected, neglecting detailed momentum conservation.

As discussed and shown in [6], the deformation potentials for acoustic and nonpolar optical phonons have been adjusted to match the experimental curves for the electron's and hole's drift velocity as function the applied electric field [35], [36], [37], [38] with FBMC transport simulations for looping boundary conditions (Fig. 1a). The matrix elements $T_{ii,e}$ and $T_{ii,h}$ for impact ionization, instead, have been chosen so that the scattering rates are consistent with the results reported by other authors [39], [40], [41], as shown in Fig. 17. The parameters used for the computation of the scattering rates in GaAs are reported in Tab. IV.

REFERENCES

[1] R. J. McIntyre, "Multiplication noise in uniform avalanche diodes," *IEEE Trans. Electron Devices*, vol. ED-13, no. 1, pp. 164–168, Jan. 1966, doi: 10.1109/T-ED.1966.15651.

[2] R. B. Emmons, "Avalanche-photodiode frequency response," *J. Appl. Phys.*, vol. 38, no. 9, pp. 3705–3714, Aug. 1967, doi: 10.1063/1.1710199.

[3] G. M. Dunn, G. J. Rees, J. P. R. David, S. A. Plimmer, and D. C. Herbert, "Monte Carlo simulation of impact ionization and current multiplication in short GaAs diodes," *Semicond. Sci. Technol.*, vol. 12, no. 1, pp. 111–120, Jan. 1997, doi: 10.1088/0268-1242/12/1/019.

[4] D. S. Ong, K. F. Li, G. J. Rees, G. M. Dunn, J. P. R. David, and P. N. Robson, "A Monte Carlo investigation of multiplication noise in thin p^+-i-n^+ GaAs avalanche photodiodes," *IEEE Trans. Electron Devices*, vol. 45, no. 8, pp. 1804–1810, Aug. 1998, doi: 10.1109/16.704382.

[5] D. S. Ong, K. F. Li, S. A. Plimmer, G. J. Rees, J. P. R. David, and P. N. Robson, "Full band Monte Carlo modeling of impact ionization, avalanche multiplication, and noise in submicron GaAs p^+-i-n^+ diodes," *J. Appl. Phys.*, vol. 87, no. 11, pp. 7885–7891, 2000, doi: 10.1063/1.373472.

[6] A. Pilotto *et al.*, "Full-band Monte Carlo simulations of GaAs p-i-n avalanche photodiodes: What are the limits of nonlocal impact ionization models?" in *Proc. Int. Conf. Simul. Semiconductor Processes Devices (SISPAD)*, Sep. 2020, pp. 1–4, doi: 10.23919/SISPAD49475.2020.9241632.

[7] M. M. Hayat, W. L. Sargeant, and B. E. A. Saleh, "Effect of dead space on gain and noise in Si and GaAs avalanche photodiodes," *IEEE J. Quantum Electron.*, vol. 28, no. 5, pp. 1360–1365, May 1992, doi: 10.1109/3.135278.

[8] R. J. McIntyre, "A new look at impact ionization—Part I: A theory of gain, noise, breakdown probability, and frequency response," *IEEE Trans. Electron Devices*, vol. 46, no. 8, pp. 1623–1631, Aug. 1999, doi: 10.1109/16.777150.

[9] C. Nichetti *et al.*, "An improved nonlocal history-dependent model for gain and noise in avalanche photodiodes based on energy balance equation," *IEEE Trans. Electron Devices*, vol. 65, no. 5, pp. 1823–1829, May 2018, doi: 10.1109/TED.2018.2817509.

[10] M. M. Hayat and B. E. A. Saleh, "Statistical properties of the impulse response function of double-carrier multiplication avalanche photodiodes including the effect of dead space," *J. Lightw. Technol.*, vol. 10, no. 10, pp. 1415–1425, Oct. 1992, doi: 10.1109/50.166785.

[11] P. Yuan *et al.*, "A new look at impact ionization—Part II: Gain and noise in short avalanche photodiodes," *IEEE Trans. Electron Devices*, vol. 46, no. 8, pp. 1632–1639, Aug. 1999, doi: 10.1109/16.777151.

[12] D. S. Ong, A. H. Tan, K. Y. Choo, K. H. Yeoh, and J. P. R. David, "Weibull-Fréchet random path length model for avalanche gain and noise in photodiodes," *J. Phys. D, Appl. Phys.*, vol. 55, no. 6, Nov. 2021, Art. no. 065105, doi: 10.1088/1361-6463/ac31f0.

[13] F. Rosset *et al.*, "A model for the jitter of avalanche photodiodes with separate absorption and multiplication regions," *Nucl. Instrum. Methods Phys. Res. A, Accel. Spectrom. Detect. Assoc. Equip.*, vol. 977, Oct. 2020, Art. no. 164346, doi: 10.1016/j.nima.2020.164346.

[14] J. Lauter, D. Protic, A. Forster, and H. Luth, "AlGaAs/GaAs SAM-avalanche photodiode: An X-ray detector for low energy photons," *Nucl. Instrum. Methods Phys. Res. A, Accel. Spectrom. Detect. Assoc. Equip.*, vol. 356, nos. 2–3, pp. 324–329, 1995, doi: 10.1016/0168-9002(94)01237-7.

[15] F. Capasso, W.-T. Tsang, and G. F. Williams, "Staircase solid-state photomultipliers and avalanche photodiodes with enhanced ionization rates ratio," *IEEE Trans. Electron Devices*, vol. ED-30, no. 4, pp. 381–390, Apr. 1983, doi: 10.1109/T-ED.1983.21132.

[16] M. V. Fischetti and S. E. Laux, "Monte Carlo analysis of electron transport in small semiconductor devices including band-structure and space-charge effects," *Phys. Rev. B, Condens. Matter*, vol. 38, no. 14, pp. 9721–9745, Nov. 1988, doi: 10.1103/PhysRevB.38.9721.

[17] M. L. Cohen and T. K. Bergstresser, "Band structures and pseudopotential form factors for fourteen semiconductors of the diamond and zinc-blende structures," *Phys. Rev.*, vol. 141, no. 2, pp. 789–796, Jan. 1966, doi: 10.1103/PhysRev.141.789.

[18] *Sentaurus Device User Guide, Version L-2016.03*, Synopsys, Mountain View, CA, USA, 2016.

[19] G. E. Bulman, V. M. Robbins, K. F. Brennan, K. Hess, and G. E. Stillman, "Experimental determination of impact ionization coefficients in (100) GaAs," *IEEE Electron Device Lett.*, vol. EDL-4, no. 6, pp. 181–185, Jun. 1983, doi: 10.1109/EDL.1983.25697.

[20] S. A. Plimmer, J. P. R. David, and D. S. Ong, "The merits and limitations of local impact ionization theory," *IEEE Trans. Electron Devices*, vol. 47, no. 5, pp. 1080–1088, May 2000, doi: 10.1109/16.841244.

[21] J. S. Cheong, M. M. Hayat, X. Zhou, and J. P. R. David, "Relating the experimental ionization coefficients in semiconductors to the nonlocal ionization coefficients," *IEEE Trans. Electron Devices*, vol. 62, no. 6, pp. 1946–1952, Jun. 2015, doi: 10.1109/TED.2015.2422789.

[22] D. Dolgos, "Full-band Monte Carlo simulation of single photon avalanche diodes," Ph.D. thesis, Integr. Syst. Lab., ETH Zürich, Zürich, Switzerland, 2011.

[23] D. S. Ong, G. J. Rees, and J. P. R. David, "Avalanche speed in thin avalanche photodiodes," *J. Appl. Phys.*, vol. 93, no. 7, pp. 4232–4239, Apr. 2003, doi: 10.1063/1.1557785.

[24] C. Nichetti *et al.*, "Gain and noise in GaAs/AlGaAs avalanche photodiodes with thin multiplication regions," *J. Instrum.*, vol. 14, no. 1, pp. 1–8, Jan. 2019, doi: 10.1088/1748-0221/14/01/c01003.

[25] M. K. Tsai, S. W. Tan, Y. W. Wu, Y. J. Yang, and W. S. Lour, "Improvements in direct-current characteristics of $Al_{0.45}Ga_{0.55}As$-GaAs digital-graded superlattice-emitter HBTs with reduced turn-on voltage by wet oxidation," *IEEE Trans. Electron Devices*, vol. 50, no. 2, pp. 303–309, Feb. 2003, doi: 10.1109/TED.2002.808428.

[26] V. Spagnolo, G. Scamarcio, W. Schrenk, and G. Strasser, "Influence of the band-offset on the electronic temperature of GaAs/Al(Ga)As superlattice quantum cascade lasers," *Semicond. Sci. Technol.*, vol. 19, no. 4, pp. S110–S112, Mar. 2004, doi: 10.1088/0268-1242/19/4/040.

[27] A. Pilotto *et al.*, "Modeling approaches for gain, noise and time response of avalanche photodiodes for X-ray detection," *Frontiers Phys., Radiat. Detectors Imag.*, 2022, doi: 10.3389/fphy.2022.944206.

[28] M. Ren, S. Maddox, Y. Chen, M. Woodson, J. C. Campbell, and S. Bank, "AlInAsSb/GaSb staircase avalanche photodiode," *Appl. Phys. Lett.*, vol. 108, no. 8, pp. 1–4, 2016, doi: 10.1063/1.4942370.

[29] M. Nada *et al.*, "High-speed III-V based avalanche photodiodes for optical communications—The forefront and expanding applications," *Appl. Phys. Lett.*, vol. 116, no. 14, Apr. 2020, Art. no. 140502, doi: 10.1063/5.0003573.

[30] S. D. March, A. H. Jones, J. C. Campbell, and S. R. Bank, "Multistep staircase avalanche photodiodes with extremely low noise and deterministic amplification," *Nature Photon.*, vol. 15, no. 6, pp. 468–474, May 2021, doi: 10.1038/s41566-021-00814-x.

[31] Y. Yuan *et al.*, "III-V on Silicon avalanche photodiodes by heteroepitaxy," *Opt. Lett.*, vol. 44, no. 14, pp. 3538–3541, Jul. 2019, doi: 10.1364/OL.44.003538.

[32] M. V. Fischetti, "Monte Carlo simulation of transport in technologically significant semiconductors of the diamond and zinc-blende structures. I. Homogeneous transport," *IEEE Trans. Electron Devices*, vol. ED-38, no. 3, pp. 634–649, Mar. 1991, doi: 10.1109/16.75176.

[33] W. Pötz and P. Vogl, "Theory of optical-phonon deformation potentials in tetrahedral semiconductors," *Phys. Rev. B*, vol. 24, no. 4, pp. 2025–2037, Aug. 1981, doi: 10.1103/PhysRevB.24.2025.

[34] N. Sano and A. Yoshii, "Impact-ionization model consistent with the band structure of semiconductors," *J. Appl. Phys.*, vol. 77, no. 5, pp. 2020–2025, Mar. 1995, doi: 10.1063/1.358839.

[35] P. A. Houston and A. G. R. Evans, "Electron drift velocity in n-GaAs at high electric fields," *Solid-State Electron.*, vol. 20, no. 3, pp. 197–204, Mar. 1977, doi: 10.1016/0038-1101(77)90184-8.

[36] L. H. Holway, S. R. Steele, and M. G. Alderstein, *Proc. 7th Biennial Cornell Electr. Eng. Conf.*, p. 199, 1979.

[37] V. L. Dalal, "Hole velocity in p-GaAs," *Appl. Phys. Lett.*, vol. 16, no. 12, pp. 489–491, 1970, doi: 10.1063/1.1653077.

[38] V. L. Dalal, A. B. Dreeben, and A. Triano, "Temperature dependence of hole velocity in p-GaAs," *J. Appl. Phys.*, vol. 42, no. 7, pp. 2864–2867, 1971, doi: 10.1063/1.1660641.

[39] H. K. Jung, K. Taniguchi, and C. Hamaguchi, "Impact ionization model for full band Monte Carlo simulation in GaAs," *J. Appl. Phys.*, vol. 79, no. 5, pp. 2473–2480, Mar. 1996, doi: 10.1063/1.361176.

[40] D. Harrison, R. A. Abram, and S. Brand, "Impact ionization rate calculations in wide band gap semiconductors," *J. Appl. Phys.*, vol. 85, no. 12, pp. 8178–8185, Jun. 1999, doi: 10.1063/1.370657.

[41] M. V. Fischetti, N. Sano, S. E. Laux, and K. Natori, "Full-band-structure theory of high-field transport and impact ionization of electrons and holes in Ge, Si, and GaAs," *J. Technol. Comput. Aided Des.*, pp. 1–50, 1996. [Online]. Available: https://ieeexplore.ieee.org/document/6449160, doi: 10.1109/TCAD.1996.6449160.

Alessandro Pilotto received the B.Sc., M.Sc., and Ph.D. degrees in electronic engineering from the University of Udine, Italy, in 2014, 2017, and 2021, respectively. From 2017 to 2021, he was at the University of Udine, where his research activities have been focused on the modeling of carrier transport and impact ionization in avalanche photodiodes based on III–V compound semiconductors, and on Monte Carlo transport simulations of electronic devices based on two-dimensional semiconductors. In 2021, he became a Post-Doctoral Researcher at the Centre de Nanosciences et de Nanotechnologies, Université Paris-Saclay, Palaiseau, France, where he is currently working on quantum transport simulations of single photon avalanche diodes.

David Esseni (Fellow, IEEE) was a Visiting Scientist at Bell Labs-Lucent Technologies, Murray Hill, NJ, USA, in 2000. In 2013, he was a Visiting Professor at the University of Notre Dame, Notre Dame, IN, USA, supported by a Fulbright Fellowship. He is currently a Professor of electronics at the University of Udine, Italy. He is the author of numerous articles and of six book chapters in his field of expertise, and he has delivered several invited presentations at international conferences. He is the coauthor of the book *Nanoscale MOS Transistors: Semi-Classical Transport and Applications* (Cambridge University Press, Cambridge, U.K., 2011. He is a fellow of the IEEE Electron Devices Society. He has served or is serving as a member of the technical committees in several conferences, including IEDM, IRPS, ESSDERC, and SISPAD. He was the General Chair of the SISPAD 2019. He has been an Associate Editor of IEEE TRANSACTIONS ON ELECTRON DEVICES from 2008 to 2017, as well as a Guest Editor of a few Special Issues of the IEEE TRANSACTIONS ON ELECTRON DEVICES.

Luca Selmi (Fellow, IEEE) received the Ph.D. degree in electronic engineering from the University of Bologna, Bologna, Italy, in 1992. Since 2000, he has been a Professor of electronics with the University of Udine, Udine, Italy, and then recently moved to the University of Modena and Reggio Emilia. His research interests include simulation, modeling, and characterization of nanoscale CMOS transistors and NVM, with emphasis on hot-carrier effects, quasiballistic transport, Monte Carlo simulation techniques, and with a recent twist toward nanoelectronic (bio)sensors, simulation and characterization of ISFET, and impedance spectroscopy sensors. He was a TPC Member of various conferences, including the IEEE IEDM and the IEEE Symposium on VLSI Technology, and the Editor of IEEE ELECTRON DEVICE LETTERS (EDL).

Pierpaolo Palestri (Senior Member, IEEE) received the Laurea degree in electronic engineering from the University of Bologna, Italy, in 1998, and the Ph.D. degree in electronic engineering from the University of Udine, Italy, in 2003. In 2000 and 2001, he held a post-doctoral position at Bell Laboratories, Murray Hill, NJ, USA. In 2005, he became an Associate Professor at the University of Udine. He has coauthored about 300 papers in international journals and conferences with peer review. His research interests include the modeling of carrier transport in nanoscale devices, as well as the design of integrated circuits for high-frequency applications.